FERMILAB-Conf-03/218-E

September 2003

Recent Results and Prospects for High p_T Physics at DØ

Cecilia E. Gerber[1]

University of Illinois at Chicago
e-mail: gerber@uic.edu
(for the DØ Collaboration)

Abstract. I present recent results from the DØ experiment using ≈ 50 pb^{-1} of data recorded at the center of mass energy of 1.96 TeV at the Fermilab Tevatron. In addition, I summarize prospects for high p_T physics at the Tevatron as a function of integrated luminosity.

PACS: 13.85.Lg, 14.54.Ha, 14.70.-e, 14.80.-j

1 Introduction

Run II at the Tevatron has started, and DØ has recently presented its first physics results [1] using data recorded at the new center of mass energy of 1.96 TeV. In this paper, I summarize recent results on the production of jets, W and Z bosons, top quarks, and on searches for the Higgs boson and physics beyond the Standard Model. A separate presentation [2] on the status of the Tevatron accelerator and the CDF and DØ detectors details the performance of the DØ detector, which is not included in this writeup. In addition, I will present prospects for high p_T physics at the Tevatron.

2 Studies of Jet Production

At the Tevatron energies, the dominant process in high p_T $p\bar{p}$ collisions is jet production. Within the framework of QCD, inelastic scattering between a proton and an antiproton can be described as an elastic collision between a single proton constituent and a single antiproton constituent. These constituents are called partons. After the collision, the outgoing partons manifest themselves as localized streams of particles referred to as "jets". Theoretical predictions for jet production are given by the folding of the parton scattering cross sections with experimentally determined parton density functions (pdf's). These predictions have recently improved with next–to–leading order (NLO) QCD scattering calculations [3, 4, 5] and new, accurately measured pdf's [6, 7]. Some of the questions that can be addressed with studies of jet production are testing of NLO QCD, extraction of pdf's, measuring the value of the strong coupling constant α_s, and testing quark compositeness.

2.1 Inclusive Jet Cross Section

The DØ collaboration measures the central inclusive jet cross section in $p\bar{p}$ collisions at $\sqrt{s} = 1.96$ TeV using an integrated luminosity of 34 pb^{-1}. The inclusive double differential jet cross section can be expressed as:

$$d^2\sigma/(dE_T d\eta) = (N_{Jet})/(\varepsilon \Delta E_T \Delta\eta \int Ldt)$$

where N_{Jet} is the total number of jets observed in a certain jet transverse energy E_T bin, ε is the selection efficiency, ΔE_T is the bin width, $\Delta\eta$ is the pseudorapidity range considered, and $\int Ldt$ is the integrated luminosity associated with the data set. The cross section is measured in the pseudorapidity interval $|\eta| < 0.5$. Figure 1 shows the inclusive jet cross section as measured from DØ data compared to NLO QCD [8]. The Jet Energy Scale uncertainty of approximately 9% below 200 GeV, and the 10% uncertainty on the luminosity normalization, are not included in the plot.

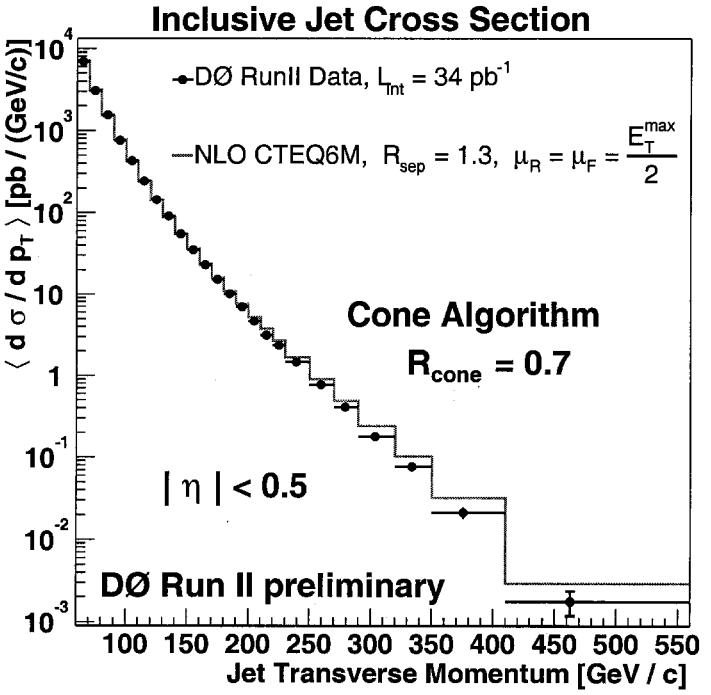

Fig. 1. Inclusive jet cross section in the central rapidity region plotted versus jet E_T. The data points are shown with statistical uncertainties, and compared to NLO QCD prediction with CTEQ6M pdf.

2.2 Dijet Production

DØ measures the jet production cross section for events with two jets as a function of the dijet invariant mass, using 34 pb^{-1} of data taken in $p\bar{p}$ collisions at $\sqrt{s} = 1.96$ TeV. The result is shown in Figure 2. The DØ data is shown with the total statistical plus systematical uncertainties added in quadrature. The 10% uncertainty on the luminosity normalization is excluded. NLO QCD [8] is in good agreement with the data.

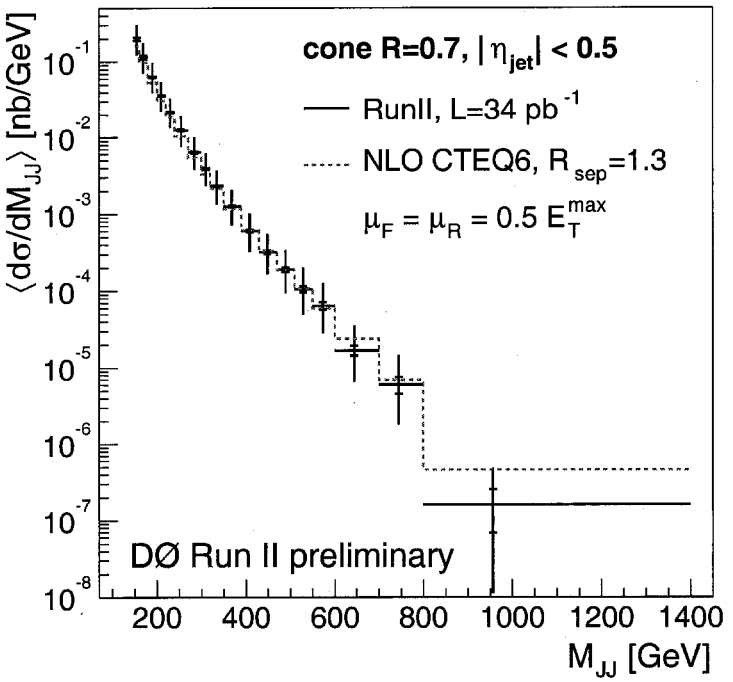

Fig. 2. Dijet cross section as a function of the dijet invariant mass. Data are shown with the stat and syst errors and compared to NLO QCD.

3 Studies of Vector Boson Production

W and Z bosons, the carriers of the weak force, are directly produced in high energy $p\bar{p}$ collisions at the Fermilab Tevatron. In addition to probing electroweak physics, the study of the production of W and Z bosons provides an avenue to explore QCD, the theory of strong interactions. Since the start of Run II, DØ has collected large numbers of W and Z bosons, both in their electronic and muonic decay channels. These samples have been very useful to benchmark the performance of the upgraded DØ detector.

27,370 $W \to e\nu$ candidates are selected from 42 pb^{-1} of data by requiring one isolated electron with $E_T > 25$ GeV, $|\eta| < 1.1$, and $\not\!\!E_T > 25$ GeV. 1139

$Z \to e^+e^-$ candidates are selected from the same data set by requiring two isolated electrons with $E_T > 25$ GeV, $|\eta| < 1.1$, and a dielectron invariant mass in the range 70 GeV $< m_{ee} <$ 110 GeV. In order to increase the statistics in this sample, no track match is required to either electron. Figure 3 shows the invariant mass distribution for the $Z \to e^+e^-$ candidates (left), and the transverse mass distribution for the $W \to e\nu$ candidates (right).

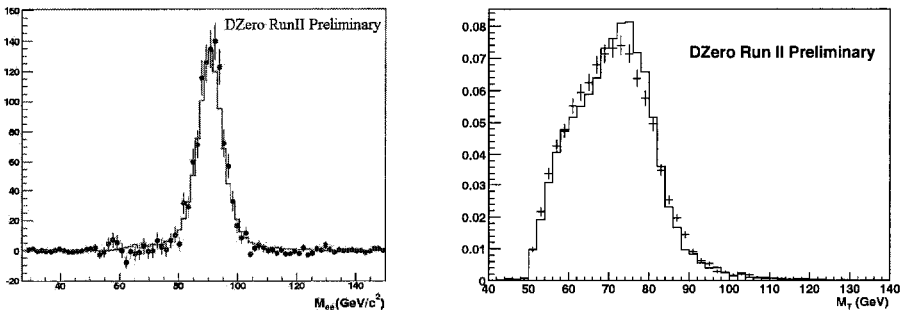

Fig. 3. The figure on the left(right) shows the dielectron invariant mass (electron+$\not\!\!E_T$ invariant mass) for 42 pb^{-1} of Run II data. The points are the background subtracted data, and the histogram is the Monte Carlo prediction from Pythia [9].

7,352 $W \to \mu\nu$ candidates are selected from a subsample of 17 pb^{-1} of data by requiring one isolated muon with $p_T > 20$ GeV, $|\eta| < 1.6$, and $\not\!\!E_T > 20$ GeV. 1585 $Z \to \mu^+\mu^-$ candidates are selected from a subsample of 32 pb^{-1} of data by requiring two oppositely-charged muons with $p_T > 15$ GeV, $|\eta|, 1.6$, and $(\Delta R)^2 = (\Delta\phi_{\mu\mu})^2 + (\Delta\eta_{\mu\mu})^2 \geq 4.0$. At least one muon was required to appear isolated both in the calorimeter and in the central tracker. To ensure a proper momentum determination, both muons are matched to a central detector track. Figure 4 shows the invariant mass distribution for the $Z \to \mu^+\mu^-$ candidates (left), and the transverse mass distribution for the $W \to \mu\nu$ candidates (right).

Using these candidate samples, DØ measures the production cross section times branching ratio for W and Z bosons in the electron and the muon channels:

$$\sigma(p\bar{p} \to W + X) \cdot B(W \to e\nu) = 3054 \pm 100(\text{stat}) \pm 86(\text{syst}) \pm 305(\text{lum}) \text{ pb}$$

$$\sigma(p\bar{p} \to Z + X) \cdot B(Z \to ee) = 294 \pm 11(\text{stat}) \pm 8(\text{syst}) \pm 29(\text{lum}) \text{ pb}$$

$$\sigma(p\bar{p} \to W + X) \cdot B(W \to \mu\nu) = 3226 \pm 128(\text{stat}) \pm 100(\text{syst}) \pm 323(\text{lum}) \text{ pb}$$

$$\sigma(p\bar{p} \to Z + X) \cdot B(Z \to \mu\mu) = 264 \pm 7(\text{stat}) \pm 17(\text{syst}) \pm 26(\text{lum}) \text{ pb}$$

The largest uncertainty in the four measurements comes from the uncertainty in the integrated luminosity, where DØ is still using the Run I value for the total $p\bar{p}$ production cross section at a lower center of mass energy. We expect the luminosity to be recalculated for the Run II center of mass energy and the uncertainty reduced in the near future. The new DØ results are in good agreement with the Standard Model expectations, as can be observed in Figure 5.

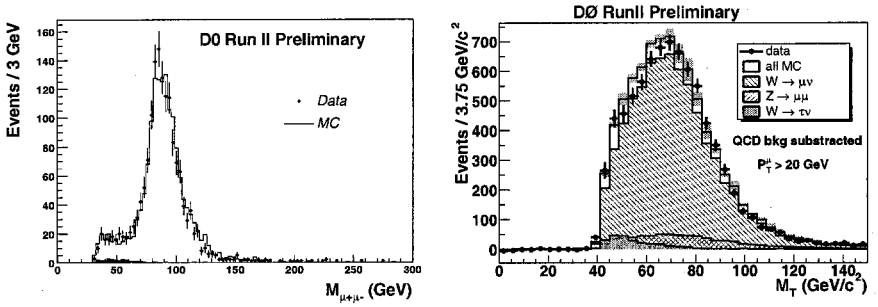

Fig. 4. The figure on the left(right) shows the dimuon invariant mass (muon+$\not\!\!E_T$ invariant mass) for 32(17) pb^{-1} of Run II data. The points are the data, compared to a parametric Monte Carlo simulation. Various sources of background are indicated in the $W \to \mu\nu$ plot, where the shaded light blue band on the Monte Carlo prediction represents the uncertainty from the detector simulation.

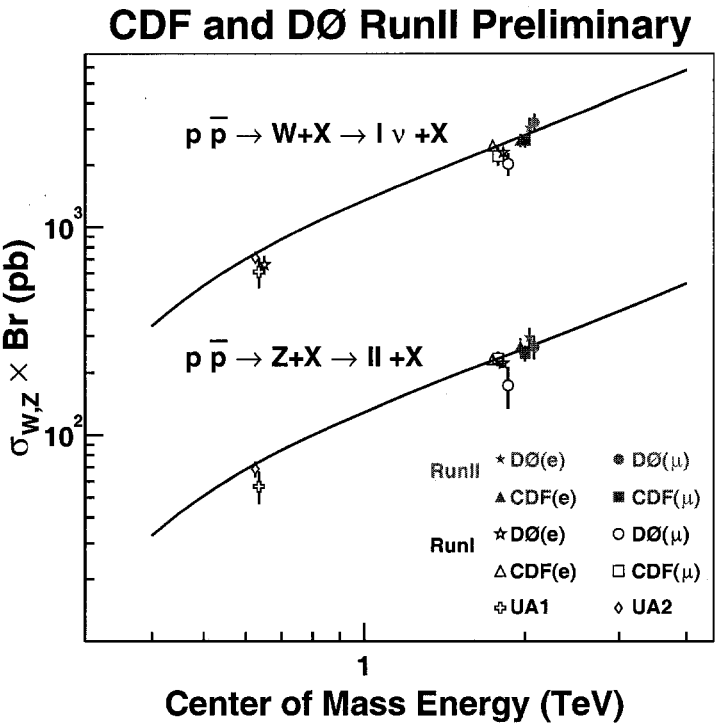

Fig. 5. $W \to l\nu$ and $Z \to l^+l^-$ cross section as a function of center of mass energy as measured by DØ and CDF, compared to the NNLO prediction [10].

4 Studies of Top quark production

At Tevatron energies, top quarks are produced predominantly in pairs. At leading order, $t\bar{t}$ production proceeds through the $q\bar{q} \to t\bar{t}$ and $gg \to t\bar{t}$ processes, with the $q\bar{q}$ process contributing 90% to the production cross section, and the gg process contributing only 10%. In the Standard Model, the top quark decays almost exclusively into a W boson and a b quark. The W boson decays into one lepton and its associated neutrino, or hadronically. Only electrons or muons are considered in the leptonic decay channels.

We have classified the $t\bar{t}$ pair decay channels as follows: the dilepton channels where both W bosons decay leptonically into an electron or a muon (ee, $\mu\mu$, $e\mu$), the lepton + jets channels where one of the W bosons decays leptonically and the other hadronically (e+jets, μ+jets), and the all-jets channel where both W bosons decay hadronically. DØ measures the $t\bar{t}$ production cross section in $\bar{p}p$ collisions at a center of mass energy of $\sqrt{s} = 1.96$ TeV in the dilepton and lepton + jets channels. These analyses are described below.

4.1 Dilepton channels

Candidate events are selected by requiring the presence of two isolated leptons, large $\not\!\!E_T$ and at least two jets. For the ee and $\mu\mu$ analyses, a tighter cut on $\not\!\!E_T$ is applied when the invariant mass of the two leptons is close to the Z boson mass window to reduce background from this source. In addition, a cut on H_t is applied, with $H_t = \Sigma(E_T^{jet} + E_T^l)$. The dominant background comes from multijet events that fake the presence of the leptons, and is estimated from data. For the ee and $\mu\mu$ channels, the background originating from $Z \to l^+l^-$ events is at a comparable level. Table 1 summarizes the result.

	$\int \mathcal{L}dt(pb^{-1})$	Background	Expected Signal	N^{obs}
ee	48	1.00 ± 0.49	0.25 ± 0.02	4
$\mu\mu$	43	0.60 ± 0.30	0.30 ± 0.04	2
$e\mu$	33	0.07 ± 0.01	0.50 ± 0.01	1

Table 1. Summary of results for the dilepton channels. The integrated luminosity for each channel is shown, together with the number of estimated background events, the number of expected $t\bar{t}$ events for a total $t\bar{t}$ production cross section of 7.0 pb, and the number of events that passed our selection cuts (N^{obs}).

4.2 lepton + jet analyses

Two approaches are used for the lepton + jet analyses: a "topological" analysis, where the selection is based entirely on kinematic variables, and a "soft lepton tag" analysis, where low p_T non-isolated muons are used to tag the presence of a jet presumably originating from a b-quark. A soft muon veto is applied to the topological analyses to ensure complete separation between the samples used in the two approaches.

The first step in the topological analysis is to select a sample enriched in W boson + jets events as a function of jet multiplicity by requiring the presence of a high p_T isolated lepton, large $\not\!\!E_T$ and at least n jets, where $n = 1, 2, 3, 4$. In addition, we veto events where a soft muon is present. We call this sample the "presample". The largest source of background to the presample comes from multijet events, where a jet fakes an electron (for the e + jets channel), and where a muon originating from the semileptonic decay of a heavy flavor quark appears isolated (for the μ + jets channel). In addition, significant $\not\!\!E_T$ due to fluctuations and mismeasurements of the jet energies fakes the presence of a neutrino. We call these instrumental backgrounds "multijet background", and estimate their contribution directly from data.

The amount of multijet background in the presample is determined as a function of jet multiplicity by first defining a "loose" sample with events that pass the same selection criteria as the presample except that the track match (isolation) requirement is not applied for the electron (muon) + jets sample. This loose sample consists of $N_{\rm s}$ signal events and $N_{\rm b}$ multijet background events, where $N_{\rm s}$ is a combination of W + jets and top events. The presample consists of $\varepsilon_{\rm s} N_{\rm s}$ signal events and $\varepsilon_{\rm b} N_{\rm b}$ multijet background events, where $\varepsilon_{\rm s}$ and $\varepsilon_{\rm b}$ are the lepton selection efficiencies for the presample relative to the loose samples, for signal and background respectively. We obtain $\varepsilon_{\rm s}$ from the $Z \to l^+ l^-$ sample, and $\varepsilon_{\rm b}$ from events with $\not\!\!E_T < 10$ GeV. Once the multijet background contribution is subtracted from the presample, we proceed to extract the number of top candidates in the $n = 4$ jet multiplicity bin as described below.

The number of W + jets events in the $n = 4$ jet bin of the presample is evaluated assuming Berends' empirical scaling law, which relates cross sections for the n^{th} and the $(n+1)^{th}$ inclusive jet multiplicities as follows [11]:

$$\frac{\sigma[W + (n+1)\ jets]}{\sigma[W + n\ jets]} = \alpha$$

where α depends on the transverse energy and pseudo-rapidity of the jets. After subtraction of multijet background as described above, the number of W+jets events with jet multiplicity $\geq i$ is given by:

$$N_i^{\rm W+t\bar{t}} = N_1^W \times \alpha^{i-1} + f_i^{t\bar{t}} N^{t\bar{t}}$$

where $N_i^{\rm W+t\bar{t}}$ is the number of events in the presample after multijet background subtraction, N_1^W is the number of W events with at least one jet in the final state, as estimated above, and $f_i^{t\bar{t}}$ is the fraction of $t\bar{t}$ events expected to be present in the presample with a jet multiplicity $\geq i$. This fraction is computed from a Monte Carlo simulation. The values of α, N_1^W, and $N_i^{t\bar{t}}$ are obtained from a fit to the distribution of $N^{\rm W+t\bar{t}}$ for $i = 1, 2, 3, 4$. We only use the α parameter to extrapolate the number of W events in the ≥ 4 jets topology

$$N_4^W = N_1^W \times \alpha^3.$$

Figure 6 shows the result of this method for the e + jets and μ + jets channels.

The number of W events in the $n = 4$ jet bin obtained by this method is subsequently corrected by trigger efficiencies. The last step in the extraction of

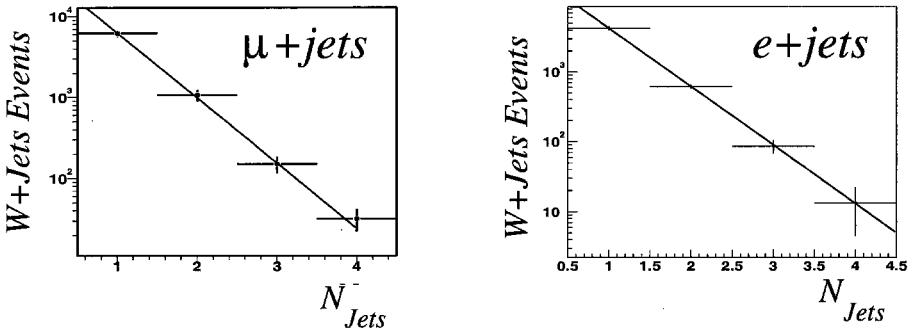

Fig. 6. Yield of inclusive $W+$ jets as a function of inclusive jet multiplicity, for the μ+jets and e+jets analyses. Note that the jet E_T and η requirements are different for the electron and muon channel, which affects the slope.

the $t\bar{t}$ signal from the overwhelming W + jets and multijet background is the application of topological cuts found to be effective in Run I [12], namely H_T and Aplanarity. Table 2 summarizes the result.

The soft lepton tag analysis starts from the same presample but requires the presence of a non-isolated, low p_T muon, and softer topological cuts. The multijet background is estimated as described above. The background from W+jets is obtained by applying a tagging probability to the presample after multijet background subtraction. The result of this analysis is also summarized in Table 2

	$\int \mathcal{L}dt(pb^{-1})$	Background	Expected Signal	N^{obs}
e + jets (topo)	50	2.7 ± 0.6	1.8	4
μ + jets (topo)	40	2.7 ± 1.1	2.4	4
e + jets (slt)	50	0.2 ± 0.1	0.5	2
μ + jets (slt)	40	0.7 ± 0.4	0.8	0

Table 2. Summary of results for the lepton + jets topological ("topo") and soft lepton tag ("slt") analyses. The integrated luminosity for each channel is shown, together with the number of estimated background events, the number of expected $t\bar{t}$ events for a total $t\bar{t}$ production cross section of 7.0 pb, and the number of events that pass our selection cuts (N^{obs}).

4.3 $t\bar{t}$ cross section measurement

Combining the results presented in the above subsections, we obtain the first measurement of the $t\bar{t}$ production cross section at a center of mass energy of 1.96 GeV using DØ data. The result

$$\sigma_{p\bar{p}\to t\bar{t}} = 8.5^{+4.5}_{-3.6} \text{ (stat) } ^{+6.3}_{-3.5} \text{ (sys) } \pm 0.8 \text{ (lumi) pb}$$

is in agreement with the Standard Model prediction, as can be seen in Figure 7. Systematic uncertainties on signal and background estimates, as well as their correlations, were accounted for in the calculation of the cross section.

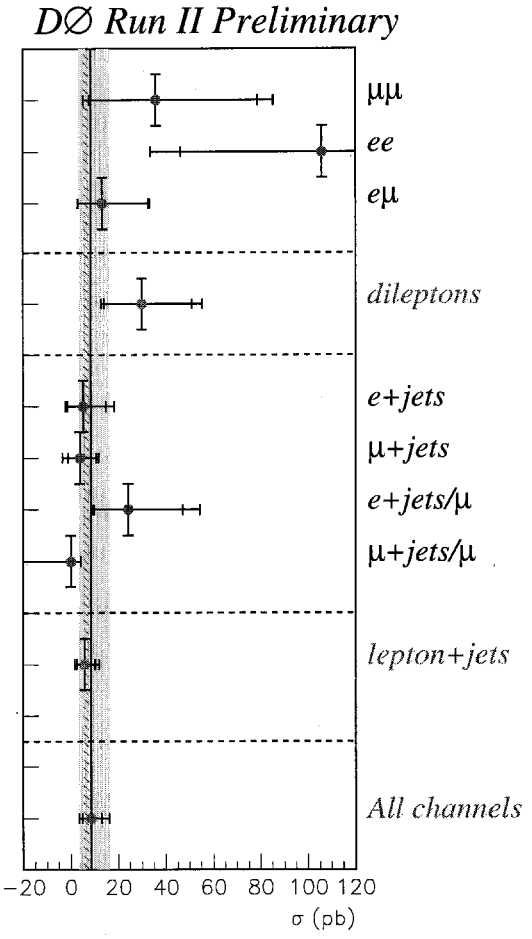

Fig. 7. Summary of individual $t\bar{t}$ production cross sections from dilepton and lepton+jets sub-combinations, and the full combination of measurements. The range of available theoretical predictions [13] is indicated by the red band.

5 Higgs Boson studies

The dominant production mode for the Standard Model Higgs boson at the Tevatron is gluon fusion $gg \to H$. However, for a light Higgs ($m_H < 140$ GeV) the dominant decay mode is $H \to b\bar{b}$, rendering this mode hopeless against the large backgrounds of $b\bar{b}$ production from other sources. In this mass range, one must look for Higgs bosons produced in association with a W or Z boson, the latter then decaying leptonically [14]. With the limited statistics currently available at the Tevatron, Higgs studies have been proceeding along two lines: background studies to Standard Model Higgs production (by studying the properties of W and Z bosons produced in association with jets), and searches relevant to extensions to the Standard Model that predict enhancements to various Higgs boson channels.

5.1 Search for $h \to \gamma\gamma$

We search for a light Higgs boson decaying into two photons $h \to \gamma\gamma$ assuming an enhanced branching fraction into photons [15]. The analysis is based on 52 pb^{-1} of data. We require 2 isolated electromagnetic objects, without a track match, and with $E_T > 25$ GeV. In addition, we apply a cut on the invariant mass of the $\gamma\gamma$ pair, which selects a region about a hypothesized Higgs mass. The largest background comes from multijet events and Z boson decays, and we estimate them from collider data using measurements of the tracking inefficiency, and the electron and photon fake rates. Figure 8 shows that there is good agreement for the diphoton invariant mass as measured by DØ, and the backgrounds predicted from collider data.

5.2 Search for $H \to WW^* \to l^+\nu l^-\nu$

Within the Standard Model, the dominant Higgs boson decay mode for Higgs masses above 135 GeV is $H \to WW^*$. Although the Standard Model event rates are expected to be too low to be observed with the current data set, alternative scenarios exist, in which either the production cross section or the branching fraction into W pairs, is enhanced [16, 17]. We search for Higgs boson decays into W pairs for which the W bosons have subsequently decayed leptonically. The main backgrounds come from multijet, $Z \to l^+l^-$, WW, W and Z + jets, and $t\bar{t}$ events. The opening angle between the two charged leptons is a useful discriminating variable between the Higgs signal and the backgrounds (in particular for the irreducible background arising from WW production), given that the two leptons from the $H \to WW^*$ decay tend to move parallel due to spin correlations. Table 3 summarizes the events that pass our selection. Combining the ee and $e\mu$ channels, we can set an upper limit at the 95% C.L. for the cross section times branching ratio of $H \to WW \to l\nu l\nu$ versus Higgs mass. The limit is shown in Figure 9 together with the expectations from various models.

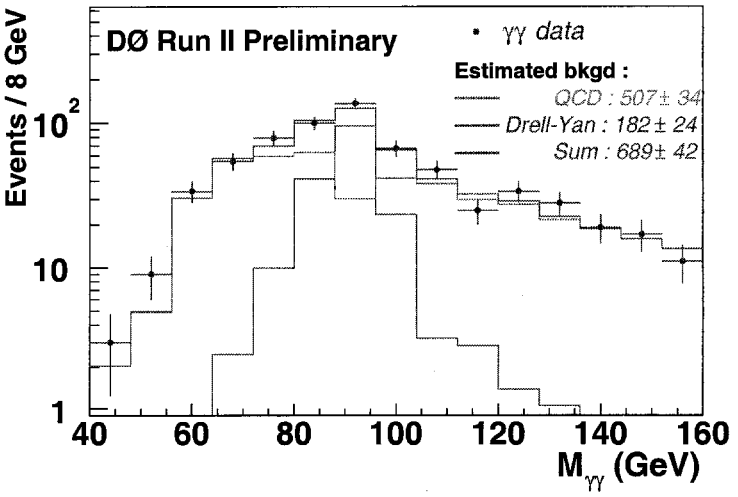

Fig. 8. Diphoton invariant mass distribution used for the $h \to \gamma\gamma$ search. Data is shown as blue crosses, and the combined Standard Model background is shown in red, with the contributions from multijet and Drell Yan shown in green and brown, respectively.

	$\int \mathcal{L}dt(pb^{-1})$	Background	N^{obs}
ee	44	0.7 ± 1.4	0
$e\mu$	34	0.9 ± 1.5	1
$\mu\mu$	48	0.3 ± 0.1	1

Table 3. Summary of results for the $H \to WW^*$ to dileptons search. The integrated luminosity for each channel is shown, together with the number of estimated background events, and the number of events that pass our selection cuts (N^{obs}). The error on the $\mu\mu$ channel is just statistical.

6 Searches for New Phenomena

Although the Standard Model is able to account for all known phenomena, it tells us nothing about the masses and mixing angles of quarks and leptons, the nature of the Higgs mechanism, or the value of the coupling constants. This proliferation of arbitrary parameters suggests the presence of new physics beyond the Standard Model. In spite of the limited amount of luminosity currently available, DØ performs searches for physics beyond the Standard Model in a variety of modes, some of which are already approaching the Run I limits. A selection of DØ Run II searches are described below.

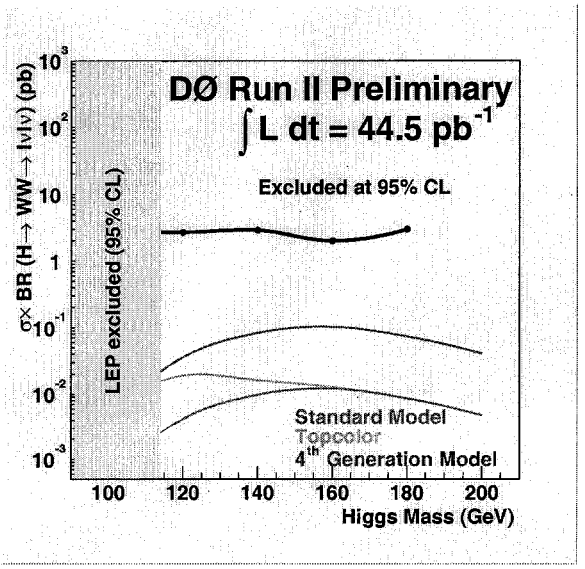

Fig. 9. 95% C.L. upper limit on the cross section times branching ratio of $H \to WW \to l\nu l\nu$ (black), together with the expectations from the Standard Model (red), Topcolor (green), and fourth generation model (blue).

6.1 Search for SUSY in trilepton final states

We perform a search for the process $\overline{p}p \to \chi_1^{\pm}\chi_2^0 \to lee\nu\chi_1^0\chi_1^0$ using 42 pb^{-1} of data by requiring the presence of two electrons, with $E_T > 15$ and 10 GeV respectively, and $\not\!\!E_T > 15$ GeV. We reduce the background originating from $Z \to e^+e^-$ events by rejecting events for which the invariant mass of the dielectron pair is close to the Z boson mass. In addition, we reject multijet background by requiring that the transverse mass of the leading electron and the $\not\!\!E_T$ be larger than 15 GeV. Our signature for the third lepton is an isolated track of at least 5 GeV. No events remain after all cuts, with a predicted Standard Model background of 0.0 ± 1.4 events and an expected SUSY signal of approximately 0.5 events in the mSUGRA (MSSM) scenario.

6.2 GMSB SUSY search

We present a SUSY search based on events with two photons and large $\not\!\!E_T$. This signature is motivated by the Gauge Mediated Supersymmetry Breaking (GMSB) model, with neutralino NLSP (Next to Lightest Supersymmetric Particle), as defined during the Snowmass-2001 workshop [18]. We analyze 42 pb^{-1} of data, and look for events with two electromagnetic objects, with no track match, and $E_T > 20$ GeV. In addition, we require that the jets in the event are of good quality (to ensure good $\not\!\!E_T$ determination, which is required to be > 30 GeV). Cuts on the opening angle between the $\not\!\!E_T$ and the leading jet further reduce backgrounds. The dominant background comes from multijet events, and is estimated from data. Figure 10 shows the number of events passing our selection

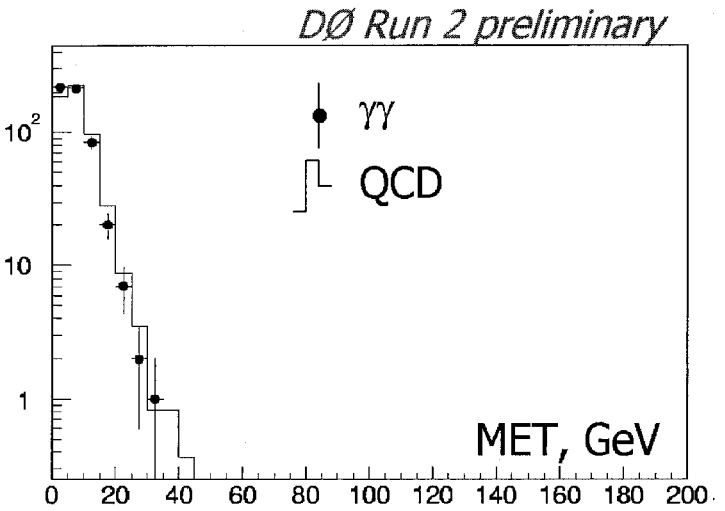

Fig. 10. The points show the number of $\gamma\gamma$ events as a function of $\not\!\!E_T$. The histogram is the expected background from multijet events.

prior to the $\not\!\!E_T$ cut as a function of $\not\!\!E_T$ compared to the expected Standard Model background. We observe good agreement between our data and the Standard Model expectation and set a limit on GMSB SUSY using the Snowmass slope [18] with Λ as the only free parameter, messenger scale mass scale $M = 2\Lambda$, number of messengers $N_5 = 1$, ratio of Higgs vev's $tan\beta = 15$, and the sign of the Higgsino mass term $\mu > 0$. This corresponds to a 95% C.L. lower limit on the neutralino mass of 66 GeV.

6.3 Scalar leptoquark searches

We perform a search for first and second generation leptoquarks using ≈ 40 pb^{-1} of data. We consider the simplest case in which leptoquarks are produced in pairs and the scalar leptoquark branching fraction to charged leptons from its own generation is equal to 1. We therefore require the presence of 2 leptons (either ee or $\mu\mu$) and 2 jets. We reject backgrounds from $Z \to l^+l^-$ by removing events with a dilepton invariant mass close to the Z boson mass, and apply additional topological cuts on the opening angle between leptons and jets. Our data is consistent with Standard Model expectations and no evidence for leptoquark production is observed. Figure 11 shows the 95% C.L. upper limit for the leptoquark cross section as a function of leptoquark mass obtained from our data. We compare our measurement in the e and μ channel with the NLO theoretical calculations for the scalar leptoquark pair production cross sections, and place an upper limit on the first and second generation scalar leptoquark cross section, respectively. Using the lower bound for the theoretical cross section band we find a lower limit on the scalar leptoquark mass of 179 GeV (first generation), and 157 GeV (second generation).

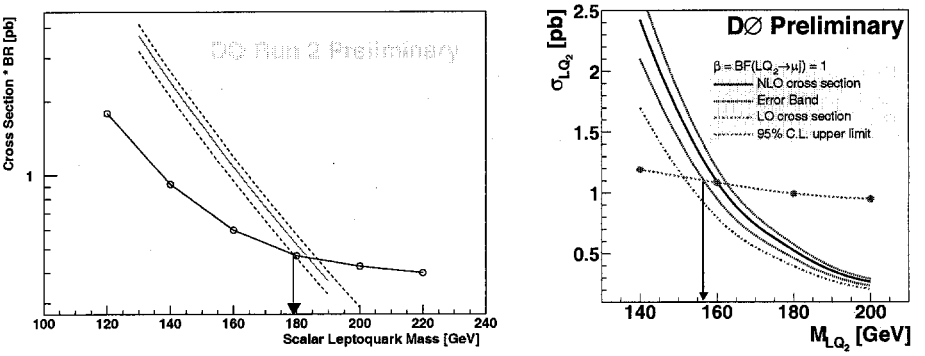

Fig. 11. Left: 95% C.L. upper limit on the first generation scalar leptoquark cross section and lower limit on the LQ mass; the black dots are the experimental limit and the red line is the NLO prediction on the cross section. Right: Same plot for second generation LQ; here the red line is the experimental limit and the black line the NLO prediction.

7 Large Extra Dimensions

We perform a search for Large Extra Dimensions (LED) following the model recently proposed by Arkani-Hamed, Dimopoulos, and Dvali (ADD) [19], in which the Standard Model particles are confined to a D3-brane, but gravity is allowed to propagate in the extra dimensions. The signature we search for is an excess of high mass dielectron, diphoton or dimuon events that arise due to the coupling to virtual gravitons. We combine the dielectron and diphoton channel (diEM) by selecting events with 2 electromagnetic objects with $E_T > 25$ GeV and no track match requirement. We veto events with more than two isolated electromagnetic objects, and require in addition $\not\!\!E_T < 25$ GeV to ensure good data quality. For the dimuon channel, we select events with 2 muons with $p_T > 15$ GeV and $M_{\mu\mu} > 40$ GeV. For both channels we estimate the instrumental backgrounds directly from data and the physics background from Monte Carlo.

The effects of Large Extra Dimensions are parameterized via a single variable $\eta_G = \frac{F}{M_s^4}$, where F is a dimensionless parameter of order ≈ 1, and η_G describes the strength of gravity in the presence of LED. We analyze the data in a plane of 2 variables that completely determine the $2 \rightarrow 2$ scattering: the invariant mass of the lepton pair and the cosine of the scattering angle in the Center of Mass frame, $cos\theta^*$. Figure 12 shows this 2-D distributions for data, backgrounds and LED signal. We then perform a 2 dimensional fit on our data in the dilepton invariant mass vs. $cos\theta^*$ plane to a combination of LED signal + background, and obtain an upper limit on the value of η_G. This limit is then translated into a 95% C.L. lower limit on the fundamental Planck scale M_S for various formalisms [20], as summarized in Table 4. The diEM limit is comparable to the DØ Run I result, and the dimuon channel is new at hadron colliders. Both results are competitive with LEP.

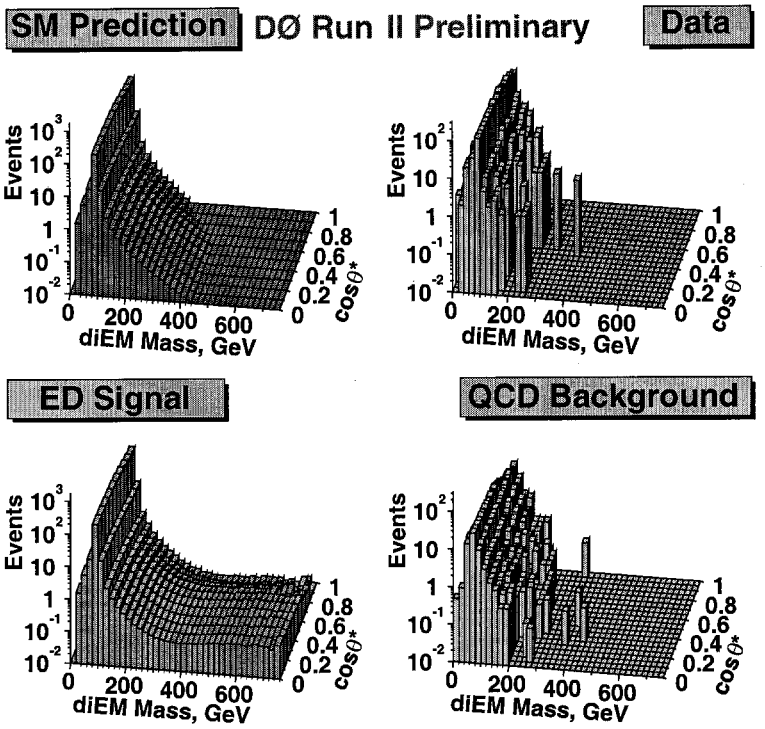

Fig. 12. diEM mass as a function of $cos\theta^*$ for Standard Model background (top left), data (top right), LED signal for $\eta_G = 2.0$ + Standard Model background (bottom left), and instrumental background (bottom right).

8 Prospects for high p_T physics at the Tevatron

Over the last years, a series of studies [21, 22, 23] have explored the potential of the Tevatron to produce physics results before the LHC becomes operational. In this section I summarize some of these expectations for a range of integrated luminosity from 300 pb^{-1} to 15 fb^{-1}. I would like to emphasize that most of the studies resulting in the predicted uncertainties and reaches mentioned below, consider the results as obtained by one detector and by extrapolating the analyses methods used in Run I. We therefore expect improvements over the quoted values by combining the results obtained by the two experiments, and by using advanced analyses techniques.

8.1 Prospects of QCD studies

QCD jet production is the dominant process in high p_T $p\bar{p}$ collisions, and as such, can be studied in detail with limited integrated luminosity. Tevatron's kinematic reach of measurements have proven to be complementary to those from other accelerators, as can be seen in Figure 13. Already in Run I, jet studies were used

	$\int \mathcal{L}dt(pb^{-1})$	GRW	HLZ, n=2	HLZ, n=7	Hewett, $\lambda = +1$
diEM	50	1.12	1.16	0.89	1
dimuon	30	0.79	0.68	0.63	0.71

Table 4. Lower limits on the fundamental Planck scale M_S in TeV as obtained from the diEM and dimuon channels for various LED formalisms.

to test QCD at higher precision, as input to PDF fits, and to set limits on quark compositeness.

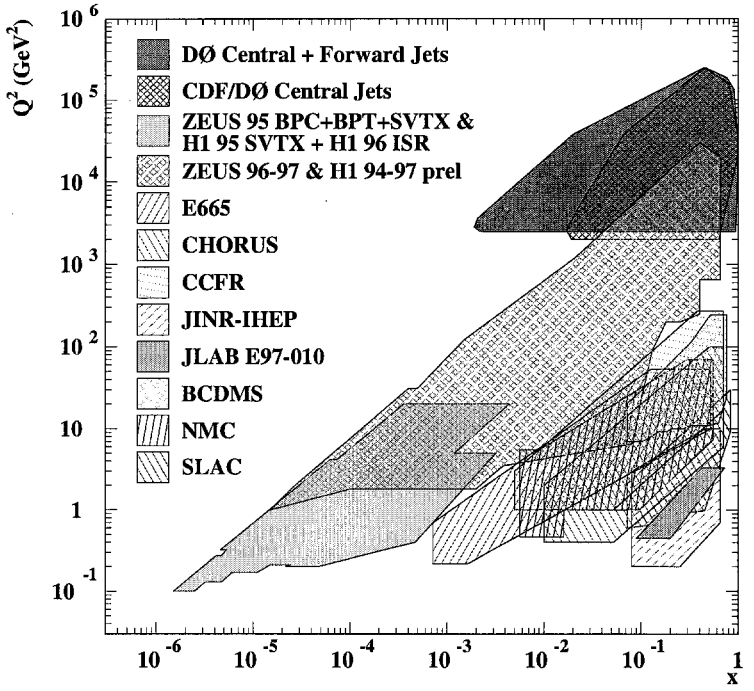

Fig. 13. Kinematic reach of measurements from different colliders and fixed target experiments in the plane of the square of the momentum transfer Q^2 vs. the parton momentum fraction x.

In addition to probing QCD, multijet background, and jets produced together with a W or a Z boson, represent the largest sources of background for any analyses involving electrons or muons + jets, like top, Higgs and searches for new phenomena. It is therefore crucial to thoroughly understand and model these processes that involve jets to reliable estimate the backgrounds to other signatures. Ongoing efforts to that effect [24] have lead to excellent opportunities for interaction between phenomenologists and experimentalists.

8.2 Prospects on Electroweak Physics

We expect significant improvements on the W boson and the top quark mass measurements, that can be used to place constrains on the Higgs boson mass. During Run I, the W boson mass measurement was performed with various methods that had different tradeoffs between statistical and systematic uncertainties. The top quark mass measurement is expected to continue to be dominated by the systematic uncertainty on the Jet Energy Scale, which might be known to a precision of less than 1 GeV using $Z \to b\bar{b}$ events. Table 5 shows expected uncertainties for the W boson and the top quark mass for 2 and 15 fb^{-1} of integrated luminosity [25]. Figure 14 shows the excluded Higgs boson mass range from the global electroweak fit using the current central values for the W boson and the top quark mass, but expected uncertainties of 20 MeV and 1 GeV, respectively.

$\int \mathcal{L}dt(pb^{-1})$	Δm_W	Δm_t (l+jets)	Δm_t (dileptons)
2 fb^{-1}	27 MeV	2.7 GeV	2.8 GeV
10 fb^{-1}	18 MeV	1.6 GeV	1.6 GeV

Table 5. Expected uncertainties for the W boson and top quark mass for two different amounts of integrated luminosity, extrapolating from uncertainties in the Run I analyses. The values are per experiment and do not include improved analyses techniques being developed [26].

8.3 Direct Searches for the Higgs Boson

The Higgs discovery potential at the Tevatron has been evaluated in depth [14] using a parameterized detector simulation that assumed averaged properties of the DØ and CDF detectors. The conclusion of the study was that a 5σ Higgs boson discovery would be possible for $m_H = 120$ GeV with a luminosity of 15 fb^{-1} from each experiment and the combination of the data from different channels. The reach on Higgs boson discovery is currently being reevaluated by both experiments. The results of this new study is expected to be ready in the near future.

8.4 Top quark Physics Program

The Tevatron collider will remain the only source of top quarks until the LHC becomes operational. The top quark was discovered in 1995 by DØ and CDF on the bases of a few tens of events. Run II gives us the opportunity to study this unique quark with an expected statistics of thousands of events, as we expect to collect $\approx$ 500 b-tagged $t\bar{t}$ events per fb^{-1} in the lepton + jets final state. The Standard Model predicts that top quarks are created via two independent production mechanisms in hadron colliders. The primary mode, in which a $t\bar{t}$ pair is produced via the strong interaction, was used by DØ and CDF to establish the existence of the top quark in 1995, and measure its mass. The second

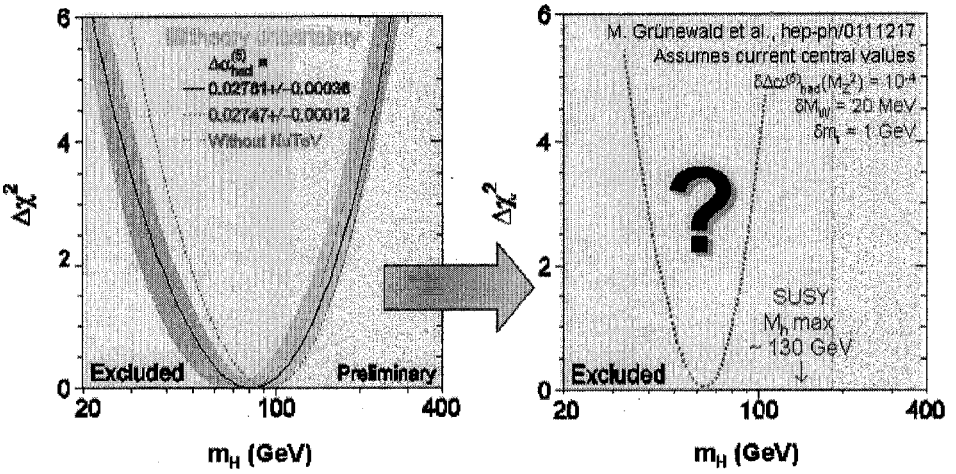

Fig. 14. Left: current indirect limit on the Higgs boson mass from the global fit to electroweak parameters. Right: expected limit on the Higgs boson mass assuming the current central values for m_W and m_t, but reduced uncertainties of 20 MeV for the W boson mass and 1 GeV for the top quark mass.

production mode of top quarks at hadron colliders is the electroweak production of a single top quark from a Wtb vertex. The predicted cross section for single top production is about half that of $t\bar{t}$ pairs, but the signal-to-background ratio is much worse. We expect to observe single top production with 1 fb^{-1} of data, in both the t and the s channel. Extracting a single top signature would be an independent confirmation of the top quark existence and a means to measure the Cabibbo-Kobayashi-Maskawa (CKM) matrix element Vtb, and study the Wtb coupling. Measuring the single top quark production cross section is also crucial in understanding the backgrounds to searches for the Higgs Boson and new physics beyond the Standard Model. Table 6 summarizes expected uncertainties on the single top production cross section and Vtb for 2 and 15 fb^{-1} of integrated luminosity [27]. In addition, we expect to measure $t\bar{t}$ spin correlations with 2 fb^{-1} of data, that would allow us to distinguish, at the 2σ level, if the top quark is indeed the spin $\frac{1}{2}$ particle the Standard Model predicts. We will also look for new physics in top production and decay, like $t\bar{t}$ mass resonances, rare and non-standard decays, and anomalous enhancements of the single top production.

8.5 Prospects of Searches beyond the Standard Model

The Tevatron is currently the only place available to directly search for supersymmetry, the most popular extension to the Standard Model. Signatures that

$\int \mathcal{L}dt(pb^{-1})$	$\Delta\sigma(s)$	$\Delta\|V_{tb}\|(s)$	$\Delta\sigma(t)$	$\Delta\|V_{tb}\|(t)$
2 fb^{-1}	21%	12%	12%	10%
10 fb^{-1}	9%	6%	5%	8%

Table 6. Expected uncertainties on the single top cross section and the extracted measurement of $|V_{tb}|$ for the s and the t single top channel, for two different amounts of integrated luminosity.

are being looked for are squarks and gluinos in channels with $\not\!\!E_T$; charginos and neutralinos in trilepton final states (which become important once the squark and gluino production reaches its kinematic limit of $\approx$ 500 GeV); gauge mediated SUSY in $\not\!\!E_T$ + photon events; and R-parity violating models. Other searches for new phenomena include leptoquarks, heavy W' and Z' bosons, and extra dimensions. We are also looking for deviations from the Standard Model in specific signatures performing quasi model independent searches, following the methods pioneered by DØ during Run I [28].

9 Conclusions

I have presented a wide range of analyses currently in progress at DØ. Several benchmark signals have been re-established, and some searches are already approaching Run I limits. And this is only the beginning. We are accumulating more luminosity, improving object identifications, and working towards more elaborate analysis methods. We believe the Tevatron physics program at Run II is rich and promising, and are enthusiastic about the physics through the end of the decade.

10 Acknowledgments

I would like to thank my DØ collaborators for their help in preparing this document. We thank the staffs at Fermilab and collaborating institutions, and acknowledge support from the Department of Energy and National Science Foundation (USA), Commissariat à L'Energie Atomique and CNRS/Institut National de Physique Nucléaire et de Physique des Particules (France), Ministry for Science and Technology and Ministry for Atomic Energy (Russia), CAPES, CNPq and FAPERJ (Brazil), Departments of Atomic Energy and Science and Education (India), Colciencias (Colombia), CONACyT (Mexico), Ministry of Education and KOSEF (Korea), CONICET and UBACyT (Argentina), The Foundation for Fundamental Research on Matter (The Netherlands), PPARC (United Kingdom), Ministry of Education (Czech Republic), A.P. Sloan Foundation, and the Research Corporation

References

1. For results presented by DØ during the spring of 2003, see the public DØ pages at http://www-d0.fnal.gov/ d0conf/2003.html

2. Jianming Qian, University of Michigan, these proceedings.
3. S. D. Ellis, Z. Kunszt, and D. E. Soper, Phys. Rev. Lett.**64**, 2121 (1990).
4. F. Aversa, *et al.* , Phys. Rev. Lett.**65**, (1990).
5. W. T. Giele, E. W. N. Glover, and D. A. Kosower, Phys. Rev. Lett.**73**, 2019 (1994).
6. H. L. Lai *et al.*Phys. Rev. D55128097.
7. A. D. Martin *et al.*, Eur. Phys. J. **C4**, 463 (1998).
8. W.T. Giele, E.W.N. Glover and D.A. Kosower, Phys. Rev. Lett. **73**, 2019 (1994).
9. H.U. Bengtsson and T. Sjorstrand, Comput. Phys. Commun. **46**, 43 (1987).
10. R. Hamberg, W.L. van Neerven and T. Matsuura, Nucl. Phys. **B359**, 343 (1991); W.L. van Neerven and E.B. Zijlstra, Nucl. Phys. **B382**, 11 (1992).
11. F. A. Berends, J. B. Tausk and W. T. Giele, "Top search in multi - jet signals," Phys. Rev. D **47**, 2746 (1993).
12. V. M. Abazov *et al.* [D0 Collaboration], Phys. Rev. D **67**, 012004 (2003)
13. E. Berger and H. Contopanagos, Phys. Rev. D57, 253 (1998). R. Bonciani, S. Catani, M. Mangano, and P. Nason, Nucl. Phys. B529, 424 (1998). N. Kidonakis, Phys. Rev. D64, 014009 (2001).
14. M. Carena, J. S. Conway, H. E. Haber, J. D. Hobbs, et al., hep-ph/0010338 (2000).
15. See, for example, S. Mrenna and J. Wells, Phys. Rev. **D63**, 015006 (2001).
16. E. Arik *et al.*, SN-ATLAS-2001-006.
17. L. Brucher, R. Santos, hep-ex/9907434.
18. P3 Summary Report, Proceedings of Snowmass 2001, Edited by N. Graf.
19. N. Arkani-Hamed, S. Dimopoulos and G. Dvali, Phys. Lett. **B429**, 263 (1998).
20. G. Giudice et al., Nucl. Phys. **B544**, 3 (1999); T. Han et al., Phys. Rev. D **59**, 105006 (1999); J. Hewett, Phys. Rev. Lett. **82**, 4765 (1999).
21. Report of the tev2000 Study Group, D. Amidei and R. Brock editors, FERMILB-Pub-96/082.
22. Run II Tevatron working group, http://fnth37.fnal.gov/run2.html
23. Testing the Standard Model at the Fermilab Tevatron, Snowmass Workshop 2001.
24. See for instance http://cepa.fnal.gov/CPD/MCTuning/index.html
25. M. Grunewald, *et al.*, hep-ph/011217.
26. See for instance the new top quark mass measurement using Run I data that represents an equivalent factor of 2.4 increase in luminosity with respect to the published result at http://www-d0.fnal.gov/%7Ed0conf/2003-talks/030425-ESTRADA-talk.ppt
27. T. Stelzer, Z. Sullivan, S. Willenbrock, Phys.Rev. **D 58**, 94021 (1998).
28. The DØ Collaboration, Phys. Rev. Lett. **86**, 3712 (2001); Phys. Rev. **D 64**, 012004 (2001).